JETIR.ORG ISSN: 2349-5162 | ESTD Year : 2014 | Monthly Issue
JOURNAL OF EMERGING TECHNOLOGIES AND INNOVATIVE RESEARCH (JETIR)
An International Scholarly Open Access, Peer-reviewed, Refereed Journal

ENHANCED VISIBLE LIGHT HYDROGEN PRODUCTION OF REDUCED GRAPHENE OXIDE INCORPORATED METAL OXIDE NANOCOMPOSITES

[1]S. Yuvarani, Dr. M.E. [2]Raja Saravanan

[1]PG and Research Department of Physics, AVS College of Arts and Science, Ramalingapuram, Salem-636106, Tamilnadu, India.

[2]Department of Physics, Government Arts College (Autonomous) Salem-636007, Tamilnadu, India.

***Abstract*:** This study presents a novel method for the synthesis of titanium dioxide (TiO_2)/reduced graphene oxide (RGO) nanocomposite photocatalyst and study the H_2 production rate under solar light. The prepared photocatalysts were analyzed for their microstructure, morphology, optical, and textural properties through XRD, TEM, Raman, UV, PL and BET analysis. XRD results suggest that both pure and RGO incorporated TiO_2 samples show anatase phase tetragonal rutile type crystalline structure. TEM pictures clearly show the spherical shaped nanoparticles of TiO_2 ranged in sizes from 30-40 nm, which are further decorated uniformly on the RGO sheets surface. When the ratio of RGO is 0.25 wt%, the highest H_2-production rate was achieved. It increased by 10-fold than bare TiO_2, reaching 1419 μmol $h^{-1}g^{-1}$ with quantum efficiency (QE) of 5.75%. The reasons were as follows. Firstly, the RGO nanosheets acted as electron acceptors. Secondly, some shallow trap states at the surface or interface of TiO_2 were created by the reduction of GO during calcination.

Keyword: TiO_2; Reduced graphene oxide: Hydrothermal; Photocatalyst; H_2 production; Solar light.

I. INTRODUCTION

Concern about the depletion of fossil fuel reserves and the pollution caused by continuously increasing energy requirements advocate the use of hydrogen gas as an energy vector, as it has the advantage of not generating pollutants or greenhouse gases when used as fuel [1]. Traditional methods for hydrogen generation, i.e., the reforming of natural gas and petroleum, require high pressures and temperatures and the use of non-renewable raw materials [2]. Therefore, the development of environmentally friendly technologies to produce hydrogen from renewable sources is becoming increasingly important. In this way, photocatalysis, which has been widely researched for the oxidation of organic pollutants [3,4], could be used to convert the technology in a cost-effective manner for hydrogen generation from renewable sources (aqueous or organic wastes) [5-9], provided high performance photocatalysts are available. Currently, TiO_2 is the most commonly used photocatalyst. However, practical applications remain limited due to its low photocatalytic efficiency, catalyst bandgap (3.2 eV), low surface area, rapid recombination rate of photogenerated electron-hole pairs and fast backward reaction between hydrogen and oxygen to generate water. Moreover, its limited visible light response, low charge carrier mobility, and high carrier recombination [10] limit the efficiency of TiO_2-based materials. Various methods such as element doping, surface modification, and heterojunction modification [11-14] have been used to improve the hydrogen production efficiency of TiO_2 - based materials.

Recently, graphene-based materials are attractive and well covered throughout out the literature [15]. Their unique 2D structure of covalently bonded carbon atoms in to a honeycomb like lattice makes them mechanically strong and conductive due to the single atomic layer. They have high surface area, which gives a high aspect ratio between the junctions and bulk components. Not much thicker are grapheme oxide or reduced graphene oxide. Recently, graphene/TiO_2 composites have re-captured broad attention in virtue of

synergetic effects between the two components. Experiments have verified the superior photocatalytic performance of TiO_2-graphene composite [16]. Similarly, Xiang and co-workers [17] also published a paper declaring the elevated photocatalytic H_2-production activity of titania nanosheets by graphene modification. Numerous investigations have indicated that the role of graphene cannot be underestimated in photocatalytic H_2 production [18]. As far as we know, reports on preparation of TiO_2/RGO form are few. This report fills this gap by designing TiO_2/RGO composite and investigating its potential in photocatalytic H_2 production.

II. RESEARCH METHODOLOGY

2.1. Materials

Tetrabutyl titanate (Analytic Reagent (A.R) 99.0%) was obtained from Sinopharm Chemical Reagent Co., Ltd. Graphite materials were purchased from Sigma Aldrich. And graphene oxide (GO) was prepared using a modified Hummers method and then dispersed into the deionized water under ultrasonic condition for 30 min.

2.2. Synthesis of TiO_2 and TiO_2/RGO composites

TiO_2/RGO was prepared by a facile hydrothermal method without using any of toxic and harsh reducing agents. Firstly, 5 mL $Ti(OC_4H_9)_4$ and 0.018 g Sodium dodecyl sulfate (SDS) were dissolved into 12 mL ethanol, stirring 30 min. Then 50 mL GO solution (0.5 mg mL^{-1}) was mixed with above mentioned solution for 3 hours sequentially until homogeneously distributed. Such mixed solution was placed into a Teflon stainless autoclave and heated 180 ^oC for 10 h. Finally, the mixture was washed several times with deionized water and ethanol, filtered, and dried in an oven at 60 ^oC. For simplicity, the as-prepared composites were designated as TG0, TG0.15, TG0.25, and TG0.5, respectively, according to the nominal weight ratio (R) of RGO to TiO_2 (i.e., 0, 0.15, 0.25, and 0.5 wt%)

2.3. Photocatalytic setup

The photocatalytic H_2 generation experiments were carried out in a 100 mL Pyrex glass reactor with flat optical entry window and external cooling jacket. 20 mL of the aqueous suspension containing 20 mg photocatalyst and sacrificial electron donor (SED) was the reaction mixture. The reactor was sealed with rubber septum and sonicated to suspend the catalyst completely in the water/SED system. Thereafter, the photoreactor was de-aerated by bubbling argon for 30 min to remove the dissolved air before light irradiation. The reaction mixture was further stirred and irradiated by a Newport Xenon lamp (Newport, USA, model no: 66924) working at 400 W with an average intensity ~ 2 Sun (0.195 W/cm^2). Intensity of the light has been measured using optical power/energy meter. The quantity of H_2 evolution was measured using N_2 as the carrier gas on a gas chromatograph (Agilent Technologies: 6890N) with TCD fitted with a 5 °A molecular sieve. The apparent quantum efficiency (AQE) was calculated according to the following equations:

AQE = number of reacted electrons/number of incident photons x 100 %
= 2 x number of evolved hydrogen molecules/number of incident photons x 100%

III. RESULTS AND DISCUSSION

3.1. Structural analysis

The structural property of the prepared photocatalyst was analyzed by XRD. Figure 1 show the powder XRD pattern of pure GO, RGO, TiO_2 and various TiO_2/RGO composite photocatalyst samples. The GO pattern shows the strong diffraction peak at 2Θ = 11.7^o (001), which corresponds to an interlayer spacing of 0.77 nm and indicate the presence of oxygen functional groups in the GO sample [19].

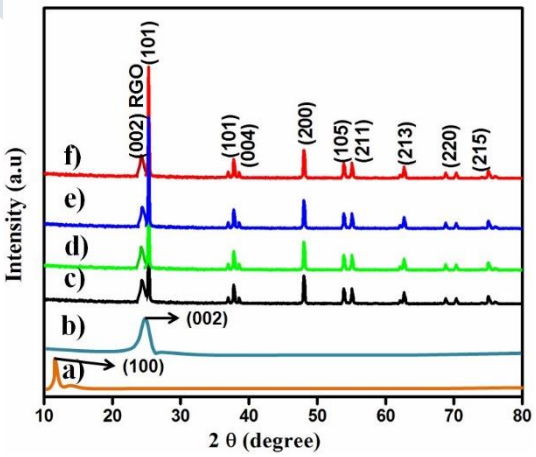

Figure 1. XRD pattern of **a)** GO; **b)** RGO; **c)** TiO_2; **d)** TG0.15; **e)** TG0.25 and **f)** TG0.5

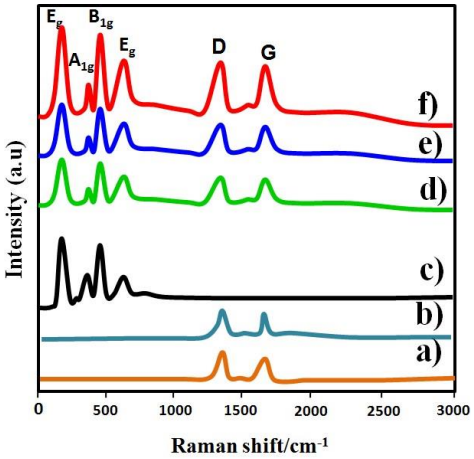

Figure 2. Raman spectra of **a)** GO; **b)** RGO; **c)** TiO_2; **d)** TG0.15; **e)** TG0.25 and **f)** TG0.5

A broad diffraction pattern of RGO is appeared at 2Θ = 25.41° (002), which corresponds to an interlayer spacing of 0.77 nm. According to the JCPDS card no. 21-1272, pure TiO_2, display the typical (101), (004), (200), (105), (211), (204), (116), (220), and (215) reflections that may be attributed to the anatase form of TiO_2. These peaks are also observed in all the TiO_2/RGO composite samples. The mixture of both TiO_2 and RGO diffraction in the composite sample is due to the successful formation of nanocomposite between them. According to the Debye Scherrer's equation [20] the grain size was calculated and the values are 17.6±0.1 nm, 17.6±0.1 nm, 17.6±0.1 nm, and 17.6±0.1 nm for TG0, TG0.15, TG0.25, and TG0.5, respectively. The Raman spectra of all the photocatalyst samples are shown in figure 2. The Raman modes of bare TiO_2 is located at 155, 401, 525 and 667 cm^{-1}, which correlated with E_g, B_{1g}, A_{1g} and E_g modes of anatase TiO_2 [21]. the Raman spectra of synthesized GO showed two peaks at the wavenumber of 1335 cm^{-1} and 1598 cm^{-1}, which corresponds to the D and G bands [22]. Both D and G bands are also appeared in the RGO sample, but the peak position of both bands are shifted towards the lower wavenumber at 1327 cm^{-1} and 1582 cm^{-1}. the shifted in the peak position is due to the re-graphitization process.

3.2. Morphological analysis

The microstructure and morphological information of the samples were examined by TEM and HRTEM. Figure 3 (a-c) shows the TEM images of RGO, TiO_2 and RGO/TiO_2 (TG0.5), respectively. The TEM image of RGO sample clearly shows that 2D sheets like wrinkle with lamer structure morphology (Fig. 3a). The pure TiO_2 TEM picture clearly shows that spherical shaped nanoparticles with the sizes in the range of 30-40 nm (Fig. 3b). In RGO/TiO_2 composite sample, the TiO_2 nanoparticles are uniformly decorated on the surface of the RGO nanosheets (Fig. 3c). Further, the TEM image of RGO/TiO_2 (TG0.5) clearly shows the lattice fringes of clearly shows the resolved lattice fringes of 0.33 nm and 0.35 nm corresponded to the (002) planes of RGO and (101) planes of anatase TiO_2, respectively (Fig. 3d). The EDS image of RGO/TiO_2 sample clearly shows the presence of main elements like Ti, O and C (Fig. 3e).

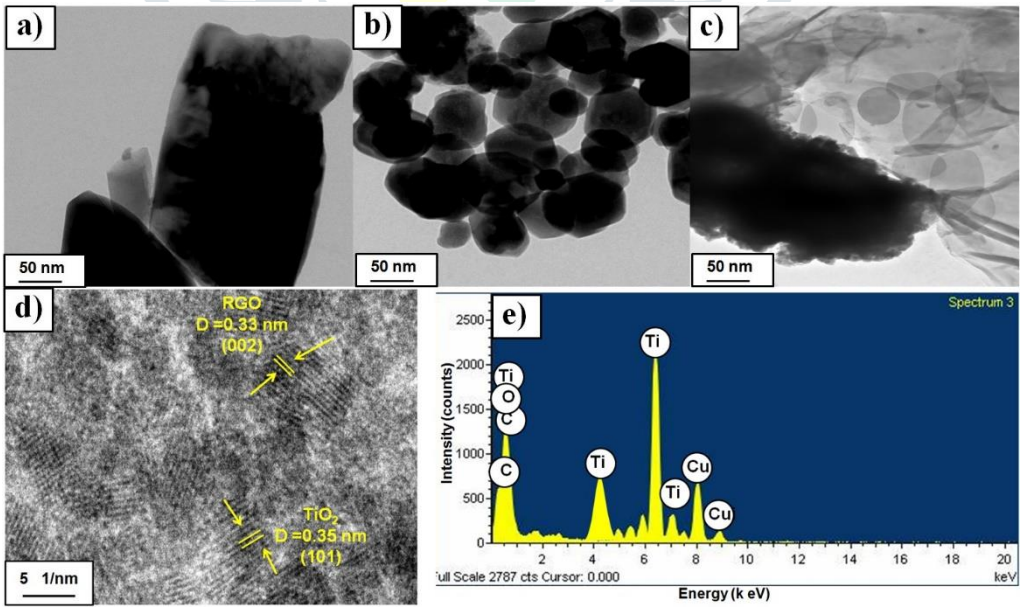

Figure 3. TEM images of **a)** RGO; **b)** TiO_2; **c)** TiO_2/RGO (TG0.5); **d)** HRTEM image of TiO_2/RGO (TG0.5) and e) EDS image of TiO_2/RGO (TG0.5)

3.3. Optical analysis

The electronic structures of TiO_2 and TiO_2/RGO composites with different amounts of RGO were researched by UV–vis absorption spectra. Figure 4a) shows the UV absorption spectra of bare TiO_2 and various composites of TiO2/RGO samples, respectively.

It was apparent that the samples had strong absorption below 400 nm (Fig. 4a), which was ascribed to the intrinsic bandgap absorption of TiO_2. Namely, electrons excited from valence band (O 2p) to conduction band (Ti 3d) [23]. The presence of RGO nanosheets resulted in slightly enhanced absorption in the visible-light range for the samples TG0.25 and TG5. A considerable red shift in the absorption edge represents the decreasing of optical band gap energy (E_g). The optical E_g was estimated from K-M formula [24-26] and found to be 3.09, 2.87, 2.67 and 2.55 eV for TG0, TG0.15, TG0.25, and TG0.5, respectively. Photoluminescence (PL) emission spectroscopy reveals the enhanced separation of photoinduced electron-hole pairs by formation of TiO2/RGO heterojunction in all the composite samples. Figure 5 shows the room temperature PL spectra of all the photocatalyst samples. PL spectra, a higher intensity in the wavelength range of 350–600 nm means easier recombination of photoinduced electron-hole pairs. Compared with pure anatase TiO_2, the recombination of photo-induced electron-hole pairs are restrained, as revealed by a weaker intensity in PL spectrum for TiO_2/RGO (Fig. 5).

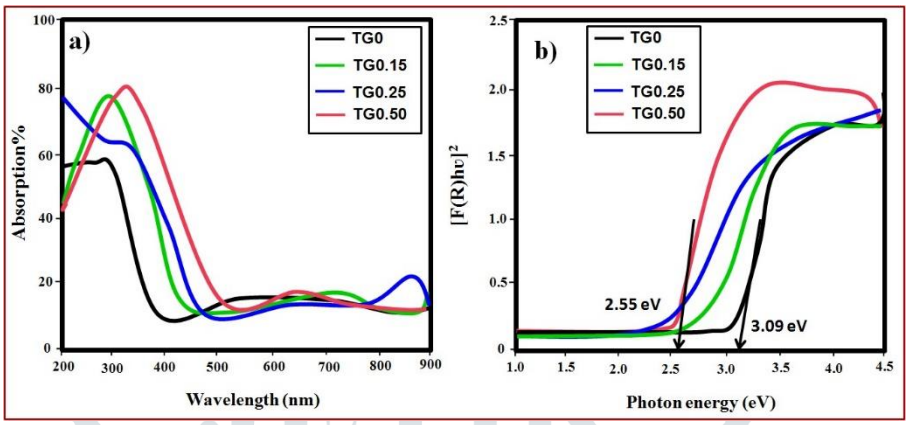

Figure 4 a) UV absorption spectra and **b)** corresponding band gap plot of all the photocatalyst samples

Particularly, TG0.5 photocatalyst has a more obvious decrease in the intensity of PL spectrum when compared with the other photocatalyst samples. The results indicate that the additional TiO_2/RGO surface heterojunction in TG0.5 plays a critical role in enhancing the separation of photo-induced electron-hole pairs, facilitating the surface reaction kinetics during photocatalytic generation of H_2.

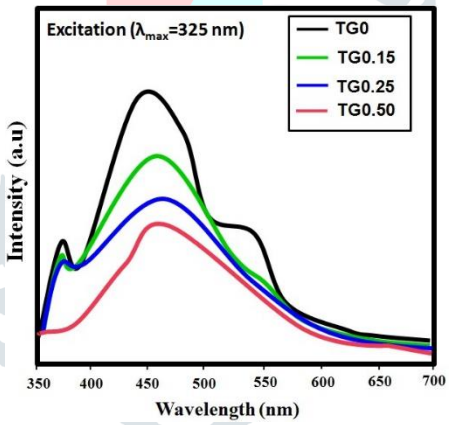

Figure 5. Room temperature photoluminescence spectrum of all the catalyst samples

3.4. Porous and surface area analysis

The nitrogen adsorption–desorption isotherms and the corresponding pore size distribution curves of TiO_2 and TG0.5 photocatalyst samples are shown in Figure 6 (a & b). As it has been reported in the previous works [27, 28], all samples have the isotherms of type IV with a typical H3 hysteresis loop, suggesting the slit-like mesoporous character of the samples. The BET surface area of TiO_2 and TG0.5 are 45.3 m^2/g and 98.4 m^2/g respectively. Similarly, the TG0.5 photocatalyst has a high porous value (17.8 nm) than compared with pure TiO_2 (12.1 nm). The TH0.5 photocatalyst exhibits a higher surface area than others, which is beneficial for the adsorption and migration of reactant and product molecules.

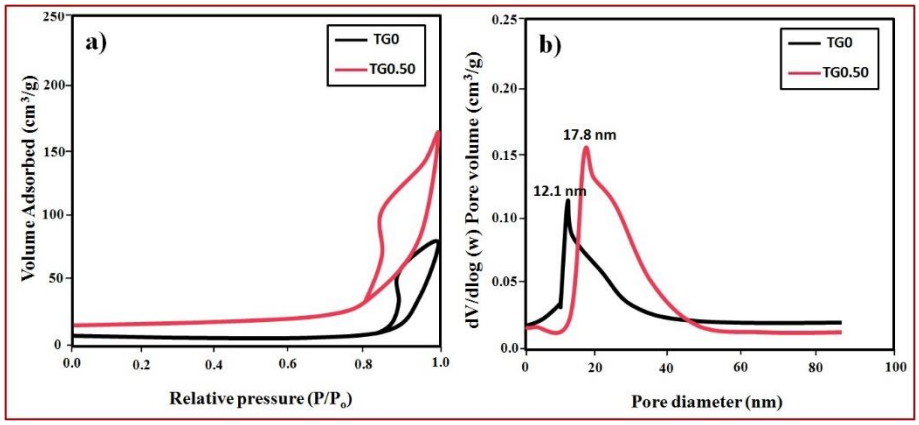

Figure 6. a) N_2 adsorption desorption and **b)** pore size distribution of pure TiO_2 and TG0.5 photocatalyst samples

3.5. H_2 evaluation analysis

Photocatalytic H_2 production efficiency of all the catalyst samples were tested under solar light and the appropriate graph is shown in Figure 7. It can be observed that the H_2 generation rate of pure TiO_2 is 345 μmol $h^{-1}g^{-1}$and apparent quantum efficiency is = 1.6%. When loaded by RGO, the H_2 generation performance of TiO_2/RGO significantly increased than compared with pure TiO_2. In particular, when the amount of RGO is 0.5wt.%, the H_2 generation efficiency of TG0.5 photocatalyst reaches the highest value of 1567 and AQY = 4.2%. From these results it can be concluded that the TiO_2/RGO exhibits and enhance performance than bare TiO_2, since it is evident their photocatalytic rate AQY efficiency. The improved photocatalytic mechanism of TiO_2/RGO is schematically expressed in Figure 8. This improvement is related to the RGO electrical properties as electron collector and to its great charge mobility, a feature that is attributed to its two-dimensional structure [29]. In in addition to this un paired π electrons of RGO make the surface interaction of TiO_2 with the RGO to extend the TiO_2 absorption range. The increase in H_2 photocatalytic ability is not only surface area enhancement.

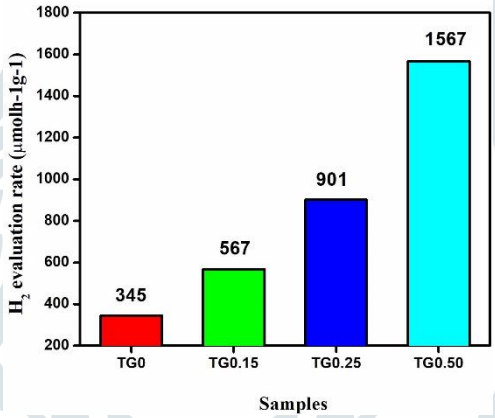

Figure 7. H_2 evaluation rate of all the photocatalyst samples

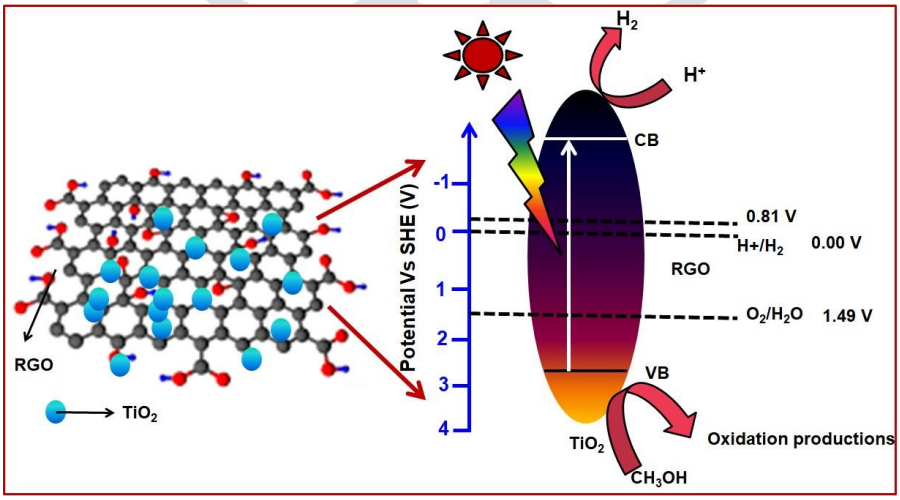

Figure 8. H_2 photocatalytic mechanism of TiO_2/RGO photocatalyst samples effect could be ascribed the conjugation of the pi bond, which make to extend the absorption of light. So, the electrons in the TiO_2 are transferred to the RGO, thus allowing a reduction in the recombination rate of charges.

IV. CONCLUSION

The effect of RGO on structural, morphological, and photocatalytic properties were systematically investigated their XRD, TEM, Raman, UV, and PL spectroscopic studies. The anatase phase TiO_2 and spherical shaped nanoparticles are identified in the XRD and TEM analysis. TiO_2 nanoparticles are further covered surface of RGO sheets in the TiO_2/RGO composite samples. The band gap energy of TiO_2 is considerably reduced and decreasing the recombination of electron – hole pairs in the pure TiO_2 after adding by RGO. When loaded by RGO, the H_2 generation performance of TiO_2/RGO significantly increased than compared with pure TiO_2. In particular, when the amount of RGO is 0.5wt.%, the H_2 generation efficiency of TG0.5 photocatalyst reaches the highest value of 1567 and AQY = 4.2%. From these results it can be concluded that the TiO_2/RGO exhibits and enhance performance than bare TiO_2, since it is evident their photocatalytic rate AQY efficiency.

REFERENCES

[1] Clarizia, L., Spasiano, D., Somma, I., Marotta, R., Andreozzi, R., and Dionysiou, D.D. 2014. Copper modified-TiO_2 catalysts for hydrogen generation through photoreforming of organics. A short review. International Journal of Hydrogen Energy, 39(30): 16812-16831.

[2] López, C.R., Melián, E.P., Méndez, J.O., Santiago, D.E., Rodríguez, J.D., and Díaz, O.G. 2015. Comparative study of alcohols as sacrificial agents in H_2 production by heterogeneous photocatalysis using Pt/TiO_2 catalysts. Journal of Photochemistry and Photobiology A: Chemistry, 312: 45-54.

[3] Van Gerben, T. Mul, G. Moulijn, J. and Stankiewicz, A. 2007. A review of intensification of photocatalytic processes. Chemical Engineering and Processing: Process Intensification, 46(9): 781-789.

[4] Spasiano, D., Marotta, R., Malato, S., Fernandez-iba~nez, P., and Di Somma. 2015. Solar photocatalysis: Materials, reactors, some commercial, and pre-industrialized applications. A comprehensive approach. Applied Catalysis B: Environmental, 170: 90-123.

[5] Montini, T., Monai, M., Beltram, A., Romero-Ocana, I., and Fornasiero, P. 2016. H2 production by photocatalytic reforming of oxygenated compounds using TiO_2-based materials. Materials Science in Semiconductor Processing, 42: 122-130.

[6] Nomikos, G.N., Panagiotopoulou, P., Kondarides, D.I., and Verykios, X.E. 2014. Kinetic and mechanistic study of the photocatalytic reforming of methanol over Pt/TiO_2 catalyst. Applied Catalysis B: Environmental, 146: 249-257.

[7] Fu, X., Long, J., Wang, X., Leung, D.Y., Ding, Z., Wu, L., Zhang, Z., Li, Z. and Fu, X. 2008. Photocatalytic reforming of biomass: A systematic study of hydrogen evolution from glucose solution. International Journal of Hydrogen Energy, 33(22): 6484-6491.

[8] Zhang, L., Xi, Z., Xing, M., and Zhang, J. 2013. Effects of the preparation order of the ternary P25/GO/Pt hybrid photocatalysts on hydrogen production. International journal of hydrogen energy, 38(22): 9169-9177.

[9] Badawy, M.I., Ghaly, M.Y., and Ali, M.E. 2011. Photocatalytic hydrogen production over nanostructured mesoporous titania from olive mill wastewater. Desalination, 267(2-3): 250-255.

[10] Pan, J., Jiang, Z., Feng, S., Zhao, C., Dong, Z., Wang, B., Wang, J., Song, C., Zheng, Y. and Li, C. 2018. The enhanced photocatalytic hydrogen production of the fusiform g-C_3N_4 modification $CaTiO_3$ nano-heterojunction. International Journal of Hydrogen Energy, 43(41): 19019-19028.

[11] Lin, S., Bai, X., Wang, H., Wang, H., Song, J., Huang, K., Wang, C., Wang, N., Li, B., Lei, M. and Wu, H. 2017. Roll-to-roll production of transparent silver-nanofiber-network electrodes for flexible electrochromic smart Windows. Advanced materials, 29(41): 1703238.

[12] Pan, J., Chi, C., You, M., Jiang, Z., Zhao, W., Zhu, M., Song, C., Zheng, Y. and Li, C. 2018. The three dimensional Z-scheme Ag_3PO_4/Ag/MoS_2/TiO_2 nano-heterojunction and its sunlight photocatalytic performance enhancement. Materials Letters, 227: 205-208.

[13] He, X., Luan, S.Z., Wang, L., Wang, R.Y., Du, P., Xu, Y.Y., Yang, H.J., Wang, Y.G., Huang, K. and Lei, M. 2019. Facile loading mesoporous Co_3O_4 on nitrogen doped carbon matrix as an enhanced oxygen electrode catalyst. Materials Letters, 244: 78-82.

[14] Yu, J., Chen, Z., Chen, Q., Wang, Y., Lin, H., Hu, X., Zhao, L. and He, Y. 2018. Giant enhancement of photocatalytic H_2 production over $KNbO_3$ photocatalyst obtained via carbon doping and MoS_2 decoration. International Journal of Hydrogen Energy, 43(9): 4347-4354.

[15] Zhang, W., Hu, Y., Yan, C., Hong, D., Chen, R., Xue, X., Yang, S., Tian, Y., Tie, Z. and Jin, Z. 2019. Surface plasmon resonance enhanced direct Z-scheme TiO_2/ZnTe/Au nanocorncob heterojunctions for efficient photocatalytic overall water splitting. Nanoscale, 11(18): 9053-9060.

[16] Zhang, H., Lv, X., Li, Y., Wang, Y. and Li, J. 2010. P25-graphene composite as a high performance photocatalyst. ACS nano, 4(1): 380-386.

[17] Xiang, Q., Yu, J. and Jaroniec, M. 2011. Enhanced photocatalytic H_2-production activity of graphene-modified titania nanosheets. Nanoscale, 3(9): 3670-3678.

[18] Xiang, Q. and Yu, J. 2013. Graphene-based photocatalysts for hydrogen generation. The Journal of Physical Chemistry Letters, 4(5): 753-759.

[19] Choi, Y.J., Kim, E., Han, J.W., Kim, J.H. and Gurunathan, S. 2016. A novel biomolecule-mediated reduction of graphene oxide: a multifunctional anti-cancer agent. Molecules, 21(3): 375.

[20] Parthibavarman, M., Sathishkumar, S. and Prabhakaran, S. 2018. Enhanced visible light photocatalytic activity of tin oxide nanoparticles synthesized by different microwave optimum conditions. Journal of Materials Science: Materials in Electronics, 29: 2341-2350.

[21] How, G. T. S., Pandikumar, A., Ming, H. N., & Ngee, L. H. 2014. Highly exposed {001} facets of titanium dioxide modified with reduced graphene oxide for dopamine sensing. Scientific reports, *4*(1): 5044.

[22] Kim, K. H., Yang, M., Cho, K. M., Jun, Y. S., Lee, S. B., & Jung, H. T. 2013. High quality reduced graphene oxide through repairing with multi-layered graphene ball nanostructures. Scientific reports, 3(1): 3251.

[23] Sajan, C.P., Wageh, S., Al-Ghamdi, A.A., Yu, J. and Cao, S. 2016. TiO_2 nanosheets with exposed {001} facets for photocatalytic applications. Nano Research, 9: 3-27.
[24] Parthibavarman, M., Karthik, M. and Prabhakaran, S. 2018. Facile and one step synthesis of WO3 nanorods and nanosheets as an efficient photocatalyst and humidity sensing material. Vacuum, 155: 224-232.
[25] Renukadevi, S. and Jeyakumari, A.P. 2020. A one-pot microwave irradiation route to synthesis of $CoFe_2O_4$-g-C_3N_4 heterojunction catalysts for high visible light photocatalytic activity: Exploration of efficiency and stability. Diamond and Related Materials, 109: 108012.
[26] Kumaresan, S., Vallalperuman, K., & Sathishkumar, S. 2017. A Novel one-step synthesis of Ag-doped ZnO nanoparticles for high performance photo-catalytic applications. Journal of Materials Science: Materials in Electronics, 28: 5872-5879.
[27] BoopathiRaja, R. and Parthibavarman, M. 2019. Hetero-structure arrays of $MnCo_2O_4$ nanoflakes@ nanowires grown on Ni foam: design, fabrication and applications in electrochemical energy storage. Journal of Alloys and Compounds, 811: 152084.
[28] Chen, R., Zhao, T., Wu, W., Wu, F., Li, L., Qian, J., Xu, R., Wu, H., Albishri, H.M., Al-Bogami, A.S. and El-Hady, D.A. 2014. Free-standing hierarchically sandwich-type tungsten disulfide nanotubes/graphene anode for lithium-ion batteries. Nano letters, 14(10): 5899-5904.
[29] Gao, W. 2015. The chemistry of graphene oxide. Graphene oxide: reduction recipes, spectroscopy, and applications. 61-95.